A Filtered-Equation Model for Operations and Research

R. MAINE

Commonwealth Meteorology Research Centre, Melbourne, Australia

(Manuscript received 25 May 1971, in revised form 31 August 1971)

ABSTRACT

A filtered-equation, pressure-coordinate, numerical prediction model is described in terms of the finite-difference formulations, and the processing strategy and its performance in an operational environment is discussed.

The model provides a useful degree of short-range skill, especially at 850 mb and higher where statistics indicate a superiority over the performance of manual prognoses. Results from differing initialization procedures and boundary value specifications are briefly discussed.

1. Introduction

Limited computing power presents problems for operational running of refined atmospheric prediction models and effective performance may only be reached after a large expenditure of effort on meteorological and program optimization. In addition, sparse operational data networks may offset expected gains in running the more refined models because of initial analysis uncertainties. There is, therefore, some justification in introducing a relatively simple filtered-equation model to operational prediction in a limited computing resource environment. Such simpler models can provide a useful reference for skill measurement and may also provide an expedient operational source of suitably balanced "initial" fields for starting the more sensitive complete Newtonian equation models, although in starting from similar analysis fields some numerical matching for compatibility of finite differences could be necessary. Filtered models have been reported extensively in Northern Hemisphere meteorological literature since the late 1950's, but during the early stages of development obtained only limited success (Ellsaesser, 1968). However, later models (e.g., Cressman, 1963; O'Neil, 1965) achieved improved performance applied to operational prediction.

Since that time, the development of the more refined finite-difference operators [e.g., Arakawa's (1966) energy conserving Jacobian] and the gradual advancement in the application of finite-difference techniques has revealed a need to incorporate these results in Southern Hemisphere models, and to test the applicability of the assumptions, review the theoretical bases, and make such local empirical adjustments as may be needed. A number of studies of this type have already been made in the Northern Hemisphere.

The aims here are to construct for use in the Southern Hemisphere a flexible prediction model which can be employed in operational numerical weather prognosis and analysis, running with limited computing facilities, and at the same time provide a basic model which may be applied conveniently in certain atmospheric research diagnostic studies, e.g., tracer experiments, and model comparison. It should be noted that a more comprehensive primitive equation model is already in the test and implementation stage on the computing equipment (IBM 360/65) presently available to this Centre.

2. Model description

The model is the following pressure-coordinate, filtered-equation, dry adiabatic system[1]:
Vorticity equation

$$(\nabla^2-\mu f_0/\bar{\psi})\frac{\partial\psi}{\partial t}=-J(\psi,\eta)+f\frac{\partial\omega}{\partial p}-\nabla\chi\cdot\nabla f \qquad (1)$$

Omega equation

$$\sigma\nabla^2\omega+f_0{}^2\frac{\partial^2\omega}{\partial p^2}=f_0\left\{\frac{\partial}{\partial p}[J(\psi,\eta)]-\nabla^2\left[J\left(\bar{\psi},\frac{\partial\psi}{\partial p}\right)\right]\right\} \qquad (2)$$

Balance equations

$$f\nabla^2\psi=g\nabla^2Z-\nabla\psi\cdot\nabla f \quad \text{(or)} \qquad (3)$$

$$f\nabla^2\psi=g\nabla^2Z-\nabla\psi\cdot\nabla f+2J\left(\frac{\partial\psi}{\partial x},\frac{\partial\psi}{\partial y}\right) \qquad (4)$$

[1] See the Appendix for definitions of symbols.

Boundary conditions for omega equation

$$\omega_b = J(\psi_g, P_g) - g\rho_L V_g C_D \nabla^2 \psi_g / f_0 + \rho_L f_0 \left(\frac{\partial \psi}{\partial t}\right)_L \quad (5)$$

$\omega = 0$ at highest level, $L = 1000$ mb

In the above ρ_L is the standard atmospheric density at the lowest model level and $(\partial\psi/\partial t)_L$ the streamfunction tendency at the lowest level, where ψ is constant at the lateral boundaries (gz/f_0) and ω zero at the lateral boundaries and the highest level. The streamfunction ψ_g is extrapolated downward to the standard pressure of the surface.

A variation of the above basic set of equations was put into operation successfully for six pressure levels by O'Neil (1965) and, in principle, his system resembles an earlier model, that of Saito (1963) having four levels in the vertical. The model equation energetics have been recently discussed by Haltiner (1968). The model described here is generalized to operate on individually assignable pressure levels and differs considerably in its implementation from that of O'Neil. In practice, the pressure levels match those generated by an operational automatic weather analysis system (see Maine, 1967), i.e., nominally, 1000, 850, 700, 500, 300, 200 and 100 mb, or any subset of these.

The linear balance equation was used by O'Neil for operational economy in preference to the more complete balance equation which is solved with the elliptic restriction

$$g\nabla^2 Z + f^2/2 - \nabla\psi \cdot \nabla f > 0. \quad (6)$$

Ellsaesser (1968) demonstrated some operational deficiencies in the use of (4) instead of (3) especially in the subtropical areas. On the other hand, Baumhefner (1968) and Krishnamurti (1968) successfully used the nonlinear formulation for both tropical and high-latitude integrations of a parallel but more complicated set of equations than those of (1) and (2). Haltiner (1968) showed that Eqs. (1), (2) and (3) are scale consistent without the Cressman long-wave retrogression term. In the model described here provision has been made to allow the choice of either formulation (3) or (4) with the solution to be started by (3) to allow convenience in experiments described later. A choice of grid size and projection corresponding to Australian region Lambert conformal, or hemispheric polar stereographic, is provided by optional use of projection computing systems.

The model used with the full balance equation (4) is intended only for use in 24–48 hr prediction experiments due to modeling restrictions. Also, since the formulation is not entirely energy-conserving, it would give rise to spurious development if integrated for longer periods. Lorenz (1960) has shown that if the terms containing velocity potential, χ, and the vertical advection of vorticity, $-\nabla\chi\cdot\nabla f$, $-\nabla\chi\cdot\nabla\zeta$, $-\omega\partial\zeta/\partial p$, are retained in association with the nonlinear balance equation one obtains an energy-preserving system under dry adiabatic conditions. The velocity potential for this model variation may be derived directly from the continuity equation in isobaric coordinates, i.e., where $\nabla^2\chi = -\partial\omega/\partial p$.

Alternatively, if the linear balance equation is employed, the integral constraint on vorticity is fulfilled by the inclusion only of the term $\nabla\chi\cdot\nabla f$ into the prognostic equation; this renders the system (1) and (3) almost energetically consistent (Haltiner, 1968). However, a form of Eq. (2) closely resembling the quasi-geostrophic type, i.e.,

$$\nabla^2(\sigma\omega) + f^2\partial^2\omega/\partial p^2 = \frac{f\partial}{\partial p} J(\psi,\eta) - \nabla^2\left(\bar{\mathbf{V}}\cdot\nabla\frac{\partial\psi}{\partial p}\right) + f\nabla f\cdot\frac{\partial\nabla\chi}{\partial p} - \nabla f\cdot\nabla\frac{\partial^2\psi}{\partial p\partial t}$$

has been used to evaluate the vertical motion in preference to the more complete form. This form of (2) has been adopted because of the order of magnitude of the last two terms and for reasons of computational economy, since O'Neil found it necessary to evaluate the ω field only every two prognostic hours.

3. Vorticity equation finite differences

After taking finite differences, Eq. (1) becomes

$$(\nabla^2 - q_L A)\delta\psi = [-J_*(\psi, \nabla^2\psi/A + f) + 4f_0 A F_1(\omega_L)]\delta t/4, \quad (7)$$

where $A = d^2/m^2$, d being the grid distance and m a map factor; f is the Coriolis parameter ($2\Omega\sin\phi$, $f_0 = f$ at 45S); q_L the long-wave retrogression parameter (Cressman, 1960) $0.25\ f_0/\bar{\psi}_L$, where L refers to the pressure level and the bar indicates an average value; and $F_1(\omega_L)$ the first derivative of $\omega = (\partial\omega/\partial p) = R_{L-1}\omega_{L-1} - R_L\omega_L - R_{L+1}\omega_{L+1}$ and $R_{L-1} = D_1/(D_2D_3)$, where $R_L = (D_1^2 - D_2^2)/(D_1D_2D_3)$, $R_{L+1} = D_2/(D_1D_3)$ and $D_1 = P_{L+1} - P_L$, $D_2 = P_L - P_{L-1}$, $D_3 = P_{L+1} - P_{L-1}$, is a pressure-weighted mean first derivative for two successive layers. In addition, δt is the time step, ψ the streamfunction, ∇^2 the standard one grid unit, five-point finite-difference Laplace operator $(\psi_1 + \psi_2 + \psi_3 + \psi_4 - 4\psi_0)$, J_1 the energy conserving Jacobian (Arakawa, 1966) taken over a grid unit $(J^{++} + J^{+\times} + J^{\times+})/3$, and $J_* = (4J_1 - J_2)/3$, where J_2 is the simplest operator taken over $2d$ grid units (Miyakoda 1960a).

4. Omega equation finite differences

The finite-difference approximation of Eq. (2) is

$$(\nabla^2 + KF_2)\omega = -K'\{F_1[-J_*(\psi, \nabla^2\psi/A + f)] + \nabla^2 J_1[\bar{\psi}, F_1(\psi_L)]/A\}, \quad (8)$$

where $K = f_0^2 A/S_L$; $S_L = -\alpha\partial\ln\theta/\partial p$, where θ is the potential temperature at pressure level L; $K' = f_0/(4S_L)$;

and $F_2(\omega_L)=T_{L+1}\omega_{L+1}-T_L\omega_L+T_{L-1}\omega_{L-1}$, where $T_{L+1}=2/(D_1D_3)$, $T_L=2/(D_1D_2)$, $T_{L-1}=2/(D_2D_3)$, derived assuming the first derivatives vary linearly between layers with ω zero at highest level and ω_B at the lowest level. In addition

$$\omega_B{}^t=J_2(\psi_G{}^t,P_G)/4A-[(\delta_x\psi_G{}^t)^2+(\delta_y\psi_G{}^t)^2]^{\frac{1}{2}}\times\nabla^2\psi_G{}^t g\rho_G C_D/(Af_0)+2\rho_G f_0(\psi_L{}^t-\psi_L{}^{t-\frac{1}{2}})/\delta t$$

where P_G is ground pressure, δ_x, δ_y are centered differences in grid directions, C_D the drag coefficient, ρ_G the density of air, and superscript t refers to the time step.

5. Balance equations and the effect of initial guess

From Eq. (4), we have

$$\nabla^2\psi=fA\pm[2gA\nabla^2Z+f^2A^2+B^2+C^2+D^2]^{\frac{1}{2}}. \quad (9)$$

This equation is solved subject to ellipticity conditions and the radicand non-negative. The difference terms B^2, C^2, D^2 were set up according to "method C" as proposed by Miyakoda (1960b), and the ellipticity condition was imposed only on the first cycle of the solution.

From Eq. (3), we have

$$\nabla^2\psi=g\nabla^2Z/f-[\nabla(gZ/f_0)\cdot\nabla f]/(4f), \quad (10)$$

where ∇ is the simple centered finite-difference gradient operator and f is kept constant within 5° of the equator.

The inversion procedure used to reform the z field from the ψ field was obtained by solution of

$$\nabla^2Z=[(\nabla^2\psi+fA)^2-f^2A^2-B^2-C^2-D^2]/(2gA), \quad (11)$$

which corresponds to the inversion of (9). The "inversion" of Eq. (10) was performed by solving

$$\nabla^2Z=(f\nabla^2\psi+\nabla\psi\cdot\nabla f)/g. \quad (12)$$

It was observed that the first guess applied to the solution method for (9) and some effect on the convergence (12) [occurring, in particular, if the solution to (9) was first started by solving (10) with f in the denominator of the right-hand side replaced by f_0] permitted a significant saving in time. It was found that a value of f_0 corresponding to 55S saved about 25% of the total solution cycles of (9).

6. Solution of omega equation

In the method adopted, the overall relaxation process was carried out from highest level to lowest level with a preset number of iterations in the Helmholz relaxation procedure allowed at each level before proceeding to the next. At each level the forcing function on the right-hand side of (8) was evaluated initially once during the entire solution. The Helmholz term $KF_2(\omega_L)$ in (8) was initially computed at each level and then subsequently changed during a relaxation using the variational relationship

$${}^{i+1}KF_2(\omega_L)={}^{i}[KF_2(\omega_L)]-K{T_L}^{i}[\delta\omega], \quad (13)$$

where i refers to the iteration number and $\delta\omega$ the variation in ω resulting from its relaxation. This procedure contrasts with an alternative method (Haltiner, 1963) in which the forcing function is re-evaluated as each level is processed.

The initial "guess" used for the vertical motion calculation was zero at the initial time. Thereafter, during prognosis, the value at the time of the last solution was used as the guess field.

7. Implementation of internal boundaries

In the "p" coordinate system it is appropriate to make a computation for boundary vertical velocities, and to allow a variable internal lower boundary because of topographic intersections with pressure levels in the solution of the three-dimensional omega equation (8).

The second derivative calculation in (8) was adjusted by the following method when the terrain level was present in the layer immediately below the level of relaxation. The value of ω computed from (5) was applied at the estimated ground pressure in the solution of (8). The field of ground pressure was calculated from the 1000-mb surface using a standard temperature, and, if the topography intersected the pressure level on which relaxation of (8) was being carried out, a value of ω_b was fixed at the internal boundary grid points and no computation of ω was carried out at points within the terrain.

In the prognosis equation (7), internal boundaries were again considered and the vertical motion term was only calculated where the actual terrain pressure was greater than the prognosis pressure level. At other points no evaluation for the vertical motion term was made.

8. Solution of the Poisson- and Helmholz-type equations

The Poisson equation appearing in the solution of either (9) or (10) was solved by a relaxation scheme due to Sheldon (1962) which is about 25% faster than the ordinary accelerated Libermann method. The usual iteration is divided into alternate sweeps over the grid, first treating even-numbered points and then odd-numbered points. The solution of the Helmholtz-type equations appearing in (7) and (8) were also solved by this relaxation procedure. In either the Poisson or Helmholz case, boundary conditions were of the first kind and the Laplacian operator was the most basic approximation.

The optimum overrelaxation coefficient was always taken to be given by (Miyakoda, 1960b)

$$\left.\begin{aligned} t&=\{\cos[\pi/(P-1)]+\cos[\pi/(Q-1)]\}/2\\ c&=[(4+b/2t)/2]-1\\ \lambda&=c-(c^2-1)^{\frac{1}{2}}\end{aligned}\right\}, \quad (14)$$

where λ is the overrelaxation coefficient, b the Helmholz term, and P and Q the dimensions of the grid. With

internal boundaries one would expect the true optimum value to be different from (14); in practice, however, with the topography in use, no difficulty was encountered in the convergence of (8).

9. Lateral boundary tendencies for solution of the prognostic equation

When the model is operated in the Australian region the southern boundary of the grid is very active meteorologically. Consequently, in the absence of information from a wider region, there is no analytically satisfactory way of setting boundary tendencies to a true value. While the initial-trial tendency values used were zero on all lateral boundaries, these deficiencies resulted in slow movement of systems near the boundary, finally accompanied by unreal distortions in the geopotential field. An attempt was made to improve the boundary tendencies for a short time (12 prognostic hours) by first introducing the observed tendencies calculated from preceding analyses and, second, by smoothly reverting to an empirical value depending on wind direction and speed. As a further development and taking a wider view, it is proposed to obtain more appropriate Australian region boundary tendencies from a geographically more extensive, probably hemispheric prediction, using this or another suitable model.

10. Adjustment of the computed 1000-mb tendencies

It was noted in the earliest experiments with the model that the 1000-mb (or M.S.L.) forecast was on the average much too slow. On the other hand, the 850-mb forecast was not always as slow and reflected actual translations far better. It was concluded that the reason for this was largely due to poor estimation of the $\partial\omega/\partial p$ term at the 1000-mb level. In most cases the finite-difference expression for this term at 1000 mb is effectively one-sided in contrast to the centered differences in ω used at 850 mb. However, it is suspected that values for ω_b itself are probably not sufficiently representative and give rise to considerable errors. Since the 850-mb tendency was considered to be reasonably representative, it was decided to weight this into the calculated 1000-mb tendency. After some experimentation a relative weight of 0.3 was found to give the best overall results, with improvements in the speed of movement of M.S.L. features.

11. Introduction of diurnal change

During the summer season over the Australian region diurnal changes are easily observed in the geopotential field particularly in the center of the continent. A diurnal cycle was therefore introduced into the predictions, using as a basis monthly statistical aspects of the diurnal change. A pre-computed diurnal change in the streamfunction was then simply added to the streamfunction computed at the end of each time step; this allowed for the possibility of some interaction between this tendency and the synoptic-scale development.

The procedure devised for calculation of the diurnal changes was as follows. A monthly climatological description of the temperature sounding was obtained at each grid point over land. The monthly mean diurnal cycles of temperature and pressure at the surface were then analyzed and values of the change generated at each grid point. The maximum temperature was assumed to occur at 1500 local time and the minimum temperature at 0600. A diurnally modified temperature sounding was then constructed assuming a dry adiabatic lapse rate at the time of maximum temperature and an isothermal sounding at minimum from the surface to the intersection with the climatological sounding. Sufficient data were then available to calculate a characteristic diurnal geopotential tendency (as a deviation from the mean sounding) for each hour of the day and night; this was then converted to a streamfunction tendency using the factor g/f_0.

12. Calculation of the M.S.L. pressure forecast

Although the surface pressure is estimated in the model, the lowest level actually prognosticated is the 1000-mb level. From this forecast the mean sea level (M.S.L.) pressure is calculated using an estimated mean temperature. The approximate formula used to derive the M.S.L. pressure field from the 1000-mb field was obtained from the hydrostatic relationship, i.e.,

$$\frac{\partial z}{\partial p}=\left(\frac{\partial z}{\partial p}\right)_s\frac{\bar{T}}{\bar{T}_s},$$

where subscript s refers to standard values for the layer 1000 mb to M.S.L. The formula neglects the variation of $\partial z/\partial p$ due to variation in M.S.L. pressure but this is small compared to the variation due to temperature. The ratio $\bar{T}/\bar{T}_s$ was not available directly and it was assumed that

$$\left(\frac{\bar{T}}{\bar{T}_s}\right)_{1000-850}=\left(\frac{\bar{T}}{\bar{T}_s}\right)_{1000-\text{M.S.L.}}.$$

13. Time steps

In the vorticity equation the leap-frog time-stepping scheme is employed as follows:

$$\left.\begin{aligned}&\psi_{t+\frac{1}{2}}=\psi_t+\delta\psi_t/2, && \text{starting step (uncentered)}\\ &\psi_{t+1}=\psi_t+\delta\psi_{t+\frac{1}{2}}, && \text{even steps (centered)}\\ &\psi_{t+\frac{1}{2}}=\psi_{t-\frac{1}{2}}+\delta\psi_t, && \text{odd steps (centered)}\end{aligned}\right\}.$$

Parameterization of the model allows replacement of the ψ field at the time t by the average of the $t-\frac{1}{2}$, t and $t+\frac{1}{2}$ fields after a given number of time steps, thus allowing time smoothing and avoiding any separation of the half-step and full-step solutions in

the differencing scheme. The size of the time step used on the Australian region grid of 137 n mi was 1 hr and restarting was carried out every 24 steps.

14. Map projections, grid points and pressure levels

The model was parameterized to run on either a regular square grid ($d=274$ n mi) circumscribing the equator on a polar stereographic projection for the Southern Hemisphere, or a regular square grid ($d=137$ n mi) on a Lambert conformal projection covering the Australian operational region (Maine, 1967). The dimensions of the grids were 47×47 and 38×23, respectively. The model was parameterized to work on N nominated pressure levels where a feasible N is bounded in operations by the total computing time. In this paper $N=7$ corresponded to the 1000-, 850-, 700-, 500-, 300-, 200- and 100-mb levels; however, since all these levels are available from the automatic analysis model, any subset of these levels may be nominated. This feature is of value in experiments investigating the optimum set of pressure levels for the operational model.

15. Model processing strategy

The steps in the prognosis computation of ψ for N pressure levels are set out below:

1) The projection constants, control parameters, and the initial streamfunctions [using (10)] were evaluated. For the full balance equation (9) the actual procedure used was that described by Maine (1967).

2) Initially and for every K steps ($K=2$), the parameters S_L and q_L were evaluated.

3) The leap-frog time-step sequence was started, vorticity advection and boundary vertical motion calculated, and the diagnostic ω equation (8) was solved for ω simultaneously at all levels. The velocity potential was then evaluated from the ω fields; then, for each level, the values of ω and χ were held constant for M time steps ($M=2$).

4) According to the calculated local time an appropriate diurnal change increment in the streamfunction was added to the synoptically changing values of the streamfunction every M time steps.

5) At each level (7) was solved for the streamfunction tendency and the new value of ψ computed. Every J steps ($J=24$) the ψ fields were time-smoothed and the leap-frog scheme restarted.

6) Forecast fields of inverted streamfunction and vertical motion were produced every K hours ($K=12$) and the M.S.L. pressure field derived.

Although the six-level model runs in 30 min with full diagnostics on the 360/65, an optimized (FORTRAN) program version has been prepared on the hemispheric grid. Estimates from this indicate that a similarly modified Australian region version will operate in 15 min for a 24-hr forecast.

16. Initialization alternatives

Although, as already pointed out, the use of formulation (3) is energetically more consistent than that of (4), it is of considerable interest to compare the results of both initialization schemes in the operational environment. A series of test prognoses were carried out for 24-hr forecasts using operational Australian region analyses during a meteorologically active period and it was found that the skill as measured by the S_1 skill score was consistently better by about 5–10% in a series of tests for all levels using the nonlinear form (4). The definition of S_1 was

$$S_1=100\frac{\sum(F-O)}{\sum(F,O)_{\max}},$$

where F and O indicate forecast and observed values, $(F,O)_{\max}$ indicates the greater value of either F or O, and the summation is made over all grid points in the area of verification. It should be noted that increasing skill is accompanied by decreasing numerical values of S_1. The initialization effect on the vertical velocity fields was such that smoother and apparently more realistic patterns of ω were derived using the nonlinear balance equation. Thus, it appears that use of the nonlinear balance expression results in detection and to some extent removal of initial time operational analysis uncertainties which the more economical and consistent linear form (3) is not capable of removing. This might not be the case in more exact, or more complete, analyses prepared for research purposes, where either balance may be as effective as the other, but in terms of prognosis skill for data-sparse, Australian region operational analyses, the nonlinear balance is preferred to the linear form. It was noted that although major nonlinear balance changes were made in regions of anticyclonic flow, the difference in results between the two initializations was not due entirely to application of the ellipticity criterion, for when a similar ellipticity filter was applied before linear balance, the conclusions were not altered.

17. Effect of vertical resolution

In an operational test environment, comparison runs were made for 24-hr forecasts using a three-level (1000, 500, 200 mb), a four-level (1000, 700, 500, 200 mb), and a six-level (1000, 850, 700, 500, 300, 200 mb) version of the model. It was observed that both upward and downward vertical motions were somewhat greater in the higher resolution version. Movement of systems eastward was appreciably greater and more accurate in the six-level version, resulting in higher S_1 skill scores at 24 hr, with a smaller rms forecast error in observed heights.

The results of a series of tests indicated that the six-level model, initialized by either linear balance or the nonlinear balance equation, performed about 10%

better (on the basis of S_1) than the corresponding three-level model. The gains over the four-level model were not as large (5–10%), but nevertheless worthwhile.

The variation of skill at each pressure level of the model over an extensive series of trials indicated a fairly regular change in skill (decreasing S_1) with height. However, at upper levels automatic analysis procedures allow more of the prognostic field to influence the analysis starting fields and the flow patterns are simpler, so this will affect comparisons of S_1.

The ratio of the average 500-mb skill score to the M.S.L. skill score over a series of about 30 test cases was 0.82, and the ratio of the 200-mb to the 500-mb skill score was 0.79.

18. Higher order Jacobian operators

Use of the higher order J^* form of the Jacobian in a six-level nonlinear balance model, in both the omega equation and the prognostic equations as indicated in (7) and (8), gave forecast results which verified slightly better at 24 hr for most levels, than did a corresponding arrangement using the lower order J_1. Both versions tended to move systems too slowly but the speed of movement of trough lines was slightly greater and vertical motions were also slightly greater for the J^* operator. On the average, in the comparison cases tried, slightly improved ($<5\%$ in S_1) results were achieved for the eastward movement of troughs.

However, in regions of high flow speed, particularly when this was onto the boundary, a two-grid length computational wave apparently arising from truncation error inconsistency was generated. This probably arose because when J_2 was calculated J_1, had to be used near boundary points. Since the complications of removing this effect with a special short-wave filter did not seem justified, J_1 was used operationally so as to avoid active boundary problems arising from this source.

19. Operational verification of results

The six-level model (1000, 850, 700, 500, 300, 200 mb) has been run on an operational basis using data provided from an operational automatic analysis system. The times of start of the prognosis runs were set so as to meet production deadlines for a manual prognosis system also using the numerical analysis as base. This is an important point in the nature of the verification since the model was effectively run in parallel with the manual prognostic scheme and was subject to the same real problems of incomplete data coverage. In fact, the model was occasionally under a disadvantage on this basis because critical late ship data could be quickly assimilated into a manual forecast but could not be fed into both the numerical analysis and prognosis systems in time to meet a production deadline. Unfortunately, the size of the data gaps and problems of interpretation are so large in the Southern Hemisphere as to allow a complete meteorological system (low or high) to be constructed on the basis of one or two critical ship reports or a re-interpretation of the satellite picture, when previous operational analyses would indicate otherwise.

Fig. 1 shows a time sequence of five-day means of S_1 computed for 24-hr forecasts in the Australian region, using a combination of simple persistence by way of control, manual methods, and the numerical model.

The Australian region was defined for verification purposes to be a region bounded by 15 to 55S and from 100 to 180E. However, the most southwestern eighth of this area was ignored because of the degree of analysis uncertainty. Almost all numerical grid points in the remaining area were used in the verification.

It is evident from the M.S.L. forecast comparisons that although the manual and numerical schemes have a roughly similar skill level with one or the other being superior for a time, the manual product is on average slightly better than the numerical. Also, the numerical forecasts were consistently better than persistence except during the summer period (November–January) when for some of the time both numerical and manual forecasts were below the level of the control skill. During the winter–spring period (August–November) the skill trends in the numerical product relate with persistence trends more so than the manual. It is thought that this is because the numerical forecasted movement is too small at this level (a fact often noted in day-to-day runs); however, during summer this trend disappears despite periods of more persistent weather.

At the 500-mb level the numerical products are clearly better than the manual for the period where manual scores were available. The margin of superiority of numerical over manual is greater than the margin of manual over numerical at M.S.L., and a similar pattern of relationship with persistence trends is evident. However, the gain of skill over persistence for the numerical models is considerable and consistent, again except for the summer period when there are occasional short reversions below persistence skill. As another means of providing a control forecast, a barotropic model, currently being run operationally, was compared with the baroclinic. The results indicate that there are only small differences between the two models at this level with the baroclinic skill being very slightly better than the barotropic overall. At the 300-mb level the manual forecasts were unfortunately not available for reference, but the numerical product showed similar behavior to the other levels and, overall, a gain over persistence skill.

While the other levels (850, 700, 200 mb) have not been treated in detail, there appears to be justification in suggesting that these will be significantly better than persistence and also better than manual, excluding consideration of 200 mb where information is inadequate. In particular, it has been subjectively noted that the movement of systems on the 850-mb chart is

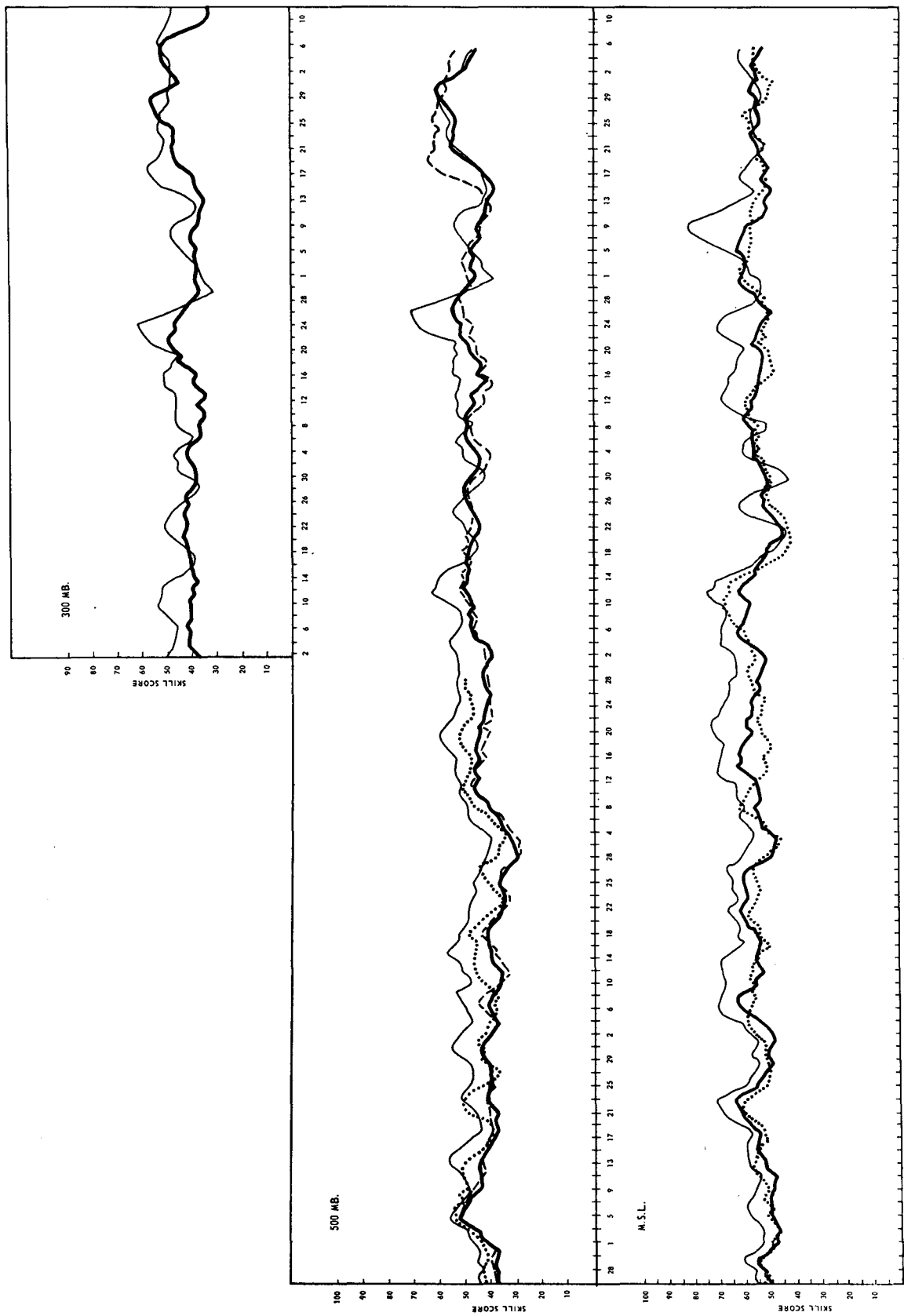

FIG. 1. Five-day moving averages of S_1 skill scores, at various levels, for 24-hr forecasts in the Australian region using simple persistence (light solid lines), manual methods (dotted lines), and two forms of the numerical model, the barotropic (dashed lines) and the baroclinic (heavy solid lines).

considerably faster than that at the surface and should result in much better relative scores than at M.S.L.

20. Future developments

In view of the significant skill in forecasting at most levels, it is proposed to develop the model further by the inclusion of a moisture equation. In the first instance this is the large-scale equation

$$\frac{\partial q}{\partial t}=-J(\psi q)-\omega\frac{\partial q}{\partial p}+AC,$$

where q is specific humidity, A a factor $[(q-q_c)/(q_s-q_c)]$, q_s the saturation value and q_c a critical value, $C=q_sT[(LR-C_pRT)/(C_pRT^2+qL^2]/p$, and $C=0$ if $q<q_c$ or $\omega\geq 0$. Thus, the diabatic heating term ∇^2Q appearing in the more complete omega equation will be able to be estimated provided an estimate of the sensible heat transfer is available. Also, it is proposed to operate a simple gross convective mechanism at each time step in order to obtain both low-level heat and moisture transfers and thus to provide improved precipitation and, consequently, wind and temperature forecasts in developing situations.

The problem of analysis uncertainties in a data-sparse region is a significant one and occasionally the omega equation refuses to converge on operational analyses after a series of prognosis steps. It is believed that under these conditions 1) the static stability may be very low for particular points or the vertical gradients of vorticity advection unreal, thus making the average stability inappropriate in the relaxation coefficient calculation, or 2) very large computed tendencies may cause spurious developments. It is proposed to carry out vertical smoothing of input analyses (e.g., Benwell and Timpson, 1968) in order to reduce vertical inconsistencies over sparse or no data regions.

21. Conclusions

An operationally viable, filtered-equation prediction model has been described which is capable of significant gains over manual operations for a large part of the atmosphere in the Australian region. The model provides forecasts of winds at several levels and is measurably better than manual, particularly at 500 mb; it is also believed to be better at 700 and 850 mb. Although true verification is hampered by uncertainties inherent in the analysis of the initial state, both in regard to actual spatial distributions and vertical slopes, the 1000-mb forecast appears to develop slower than actual when operating off the routine numerical analyses. In view of the skill available for 24-hr forecasting, it is considered that the model should also be able to provide a suitable means to cycle automatic analysis starting fields in time, thus providing dynamically consistent fields in the data-sparse regions when these are not drastically reviewed because of conflicting or new satellite data inferences.

The model itself is flexible in terms of the number and placement of levels chosen, but practical restrictions concerning vertical resolution and coupling to an operational analysis scheme govern the selection of levels.

It is considered that the model is capable of and should be developed further to include precipitation forecasts for 24-hr periods.[2]

Acknowledgments. The author is indebted to J. Young (CMRC) for much assistance in the preparation of the computer program, to R. Falconer (Bureau of Meteorology) and P. Powers (CMRC) for preparation of the programs and data for the skill score verifications, and D. Gauntlett (CMRC) for comments on the manuscript.

APPENDIX

List of Symbols

A	grid projection parameter, d^2/m^2, where d is grid distance and m the scale factor appropriate to the projection
C_D	surface drag coefficient
B,C,D	parameters defined by Miyakoda (1960) for the solution of the nonlinear balance equation
f,f_0	Coriolis parameter, an average value of f
g	gravitational acceleration
K	numerical coefficient, f_0^2S/A
K'	numerical coefficient, $f_0/(4SA)$
p,p_g	pressure, ground pressure
q	long-wave retrogression parameter
S	static stability parameter, $\alpha\partial\ \ln\theta/\partial p$
t	time coordinate
$\mathbf{V},\mathbf{V}_G$	total wind $(\mathbf{k}\times\nabla\psi+\nabla\chi)$, wind at ground pressure
Z	height of a constant pressure surface
ψ	a streamfunction, $\nabla^2\psi=\zeta$, where $\delta\psi$ is the change in ψ during an interval δt
χ	vertical potential, $\nabla^2\chi=-\partial\omega/\partial p$
ω	vertical velocity in p coordinates $(\omega=dp/dt)$
σ	static stability, $\alpha\partial\ \ln\theta/\partial p$
θ	potential temperature
α,ρ	specific volume, density of air at *STP*
ζ,η	relative vorticity, absolute vorticity

[2] *Note added in proof:* During the evaluations carried out with the model as described, it was observed that at mean sea level anticyclones tended to over develop particularly in more northern latitudes, and low pressure systems tended to fill. To a considerable extent this effect could be removed from the surface charts by a positive increase of all surface vorticities by some 10–15%; however, at high levels, the effect was hardly noticeable. It was evident that the $\mu f_0/\bar{\psi}$ term in (1) was a most likely cause of the undesirable low-level development, and in retrospect there seems little justification for including this energetically inconsistant term in a model of this type. Following the evaluation series (Fig. 1) the term was removed completely from the model with favorable results and an improvement in surface forecasts.

μ coefficient in Cressman long-wave retrogression parameter

REFERENCES

Arakawa, A., 1966: Computational design for long-term numerical integration of the equations of fluid motion: Two-dimensional incompressible flow. Part 1. *J. Comput. Phys.*, **1**, 119–143.

Baumhefner, D. P., 1968: Application of a diagnostic numerical model to the tropical atmosphere. *Mon. Wea. Rev.*, **96**, 218–227.

Benwell, G. R. R., and M. S. Timpson, 1968: Further work with the Bashby Timpson 10-level model. *Quart. J. Roy. Meteor. Soc.*, **94**, 12–24.

Cressman, G. P., 1960: Improved terrain effects in barotropic forecasts. *Mon. Wea. Rev.*, **88**, 327–342.

——, 1963: A three-level model suitable for daily numerical forecasting. N.M.C. Tech. Memo. No. 22, National Meteorological Center, NOAA, Suitland, Md.

Ellsaesser, W. H., 1968: Diagnosis of early baroclinic models. *J. Appl. Meteor.*, **7**, 153–158.

Haltiner, G. J., 1963: Computation of the large-scale vertical velocity. *J. Appl. Meteor.*, **2**, 242–259.

——, 1968: Numerical weather prediction. Tech. Rept. 30-1768-142, Naval Weather Research Facility, Norfolk, Va.

Krishnamarti, T. N., 1968: A diagnostic balance model for studies of weather systems of low latitudes and high latitudes: Rossby number less than one. *Mon. Wea. Rev.*, **96**, 197–207.

Lorenz, E. N., 1960: Energy and numerical prediction. *Tellus*, **12**, 364–373.

Miyakoda, K., 1960a: Numerical calculations of Laplacian and Jacobian using 9 and 25 grid point systems. *J. Meteor. Soc. Japan*, **38**, 94–106.

——, 1960b: Test of convergence speed of iterative methods for solving two- and three-dimensional elliptic-type differential equations *J. Meteor. Soc. Japan*, **38**, 107–123.

Maine, R., 1967: Experiments with the barotropic model in the Australian region. *Australian J. Meteor.*, **15**, 169–189.

——, and R. S. Seaman, 1967: Developments for an operational automatic weather analysis system in the Australian region. *Australian Meteor. Mag.*, **15**, 13–31.

O'Neil, H. M., 1965: The 3D Weather Wing six-level model. Air Weather Service, Scientific Services Tech. Note 14.

Saito, N., 1963: On the four-level geostrophic model. Tech. Rept. No. 2, Japan Meteorological Agency.

Sheldon, J. W., 1962: Iterative methods for the solution of elliptic partial differential equations. *Mathematical Methods for Digital Computers*, New York Wiley, 144–156.